INORGANIC CHEMISTRY FRONTIERS

RESEARCH ARTICLE

View Article Online
View Journal | View Issue

Cite this: *Inorg. Chem. Front.*, 2025, **12**, 1656

Designing a novel perovskite-type $KCd(NH_2SO_3)_3$ with deep-ultraviolet transparency and strong second-harmonic generation response†

Yujie Fan,[a,b] Li Zhong,[a,b] Haotian Tian,[b] Chensheng Lin,[b] Lingli Wu,[b] Tao Yan *[b] and Min Luo *[b]

Designing deep-ultraviolet (DUV) nonlinear optical (NLO) materials that simultaneously achieve DUV transparency and strong second-harmonic generation (SHG) remains a significant challenge. Here, we overcome this hurdle by harnessing the versatility of the perovskite (ABX_3) structure to develop a novel DUV NLO crystal. Specifically, we have successfully synthesized a non-centrosymmetric Cd-containing sulfamic compound, $KCd(NH_2SO_3)_3$, inspired by the perovskite architecture. The strategic incorporation of $SO_3NH_2^-$ groups at the X-sites not only induces distorted $[CdO_3N_3]$ octahedra, thereby enhancing the SHG response, but also ensures an ultrawide bandgap, which enables excellent DUV transparency. Consequently, this material exhibits a strong SHG response, approximately 1.1 times that of KH_2PO_4 (KDP), with a DUV cutoff edge below 190 nm. Furthermore, large transparent single crystals ($20 \times 17 \times 5$ mm^3) can be readily grown *via* a simple aqueous solution method, underscoring its potential for practical application. This innovative approach offers new design strategies for DUV NLO materials, overcoming the traditional trade-off between SHG response and UV transparency.

Received 29th November 2024,
Accepted 31st December 2024

DOI: 10.1039/d4qi03043e

rsc.li/frontiers-inorganic

Introduction

Deep-ultraviolet (DUV) nonlinear optical (NLO) crystals are pivotal in generating DUV lasers through direct frequency doubling technology, finding critical applications in advanced instrumentation, micromachining, and biogenetic engineering.[1–6] Essential criteria for these crystals include strong second-harmonic generation (SHG) performance (>1 × KDP) and a short ultraviolet absorption edge ($\lambda_{cut\text{-}off}$ < 200 nm).[7] However, these requirements often impose competing constraints, presenting a long-standing challenge in designing materials that achieve both high SHG efficiency and short UV absorption edge. Currently, $KBe_2BO_3F_2$ (KBBF)[3] is the only material suitable for DUV applications, but its reliance on toxic BeO and its layered growth habit limits its broader applicability.[8] This underscores the vital need to develop novel, practical DUV NLO crystals.

Perovskites (ABX_3), with their flexible lattice structures, inherent stability, and adaptable design capabilities,[9] have excelled in various domains such as photovoltaics,[10] catalysis,[11,12] and superconductivity.[13,14] Prominent perovskite-type oxides, including $BaTiO_3$ (λ = 400 nm),[15] $LiNbO_3$ (λ = 300 nm),[16] and $LiTaO_3$ (λ = 280 nm),[17] are classic commercial NLO materials, distinguished by their significant SHG effects and their ability to be grown as large crystals. Their robust SHG performance stems from the second-order Jahn–Teller (SOJT) effect,[18] where the distortion of $[BX_6]$ (B = Ti^{4+}, Nb^{5+}, Ta^{5+}) octahedra formed by d^0 transition metals (TMs) provides active units for SHG. Research, including studies by Ok *et al.*,[19] has revealed that these distorted octahedra enhance polariz-

[a]*College of Chemistry, Fuzhou University, Fuzhou, Fujian 350108, China*
[b]*Key Laboratory of Optoelectronic Materials Chemistry and Physics, Fujian Institute of Research on the Structure of Matter, Chinese Academy of Sciences, Fuzhou, Fujian 350002, China. E-mail: lm8901@fjirsm.ac.cn, yantao@fjirsm.ac.cn*

†Electronic supplementary information (ESI) available: Crystallographic and structure data (Tables S1–S4), and figures containing the measurement results and detail of $KCd(NH_2SO_3)_3$ (Fig. S1–S7). CCDC 2393438 for $KCd(NH_2SO_3)_3$. For ESI and crystallographic data in CIF or other electronic format see DOI: https://doi.org/10.1039/d4qi03043e

Prof. Min Luo received his B.S. in metallurgical engineering from Central South University, China, in 2011, and his Ph.D. from the Fujian Institute of Research on the Structure of Matter (FJIRSM), Chinese Academy of Sciences in 2016. In the same year, he started his independent career as an assistant professor at FJIRSM. From 2020 to 2022, he was an associate professor at FJIRSM and was promoted to full professor in 2023. He is a recipient of the National Natural Science Foundation of China Excellent Young Scientists Fund. His current research interests include the design, synthesis, and crystal growth of new nonlinear optical materials.

ability, promoting non-centrosymmetric (NCS) structures necessary for effective SHG. However, distorted octahedra constructed from d^0 TMs suffer from d–d transitions that significantly limit the bandgap, preventing classic perovskites from accessing the DUV region.[20] Thus, designing distorted octahedra within the perovskite framework to achieve DUV capabilities while maintaining strong SHG presents an intriguing and innovative research avenue.

To tackle this challenge, d^{10} transition metals, such as Zn^{2+} or Cd^{2+}, emerge as ideal B-site candidates, as they not only induce polar displacements conducive to forming distorted polyhedra but also, owing to their lack of d–d transitions, mitigate red shifts in the absorption edge.[21–23] To further amplify octahedral distortion for enhancing SHG responses and expanding the bandgap, we strategically employed X-site ligands, guided by several considerations. First, according to ligand field theory,[24] the coordination of different ligands with central atoms affects electronic configurations, leading to ligand field splitting. This process modifies the length and strength of metal–ligand bonds, creating favorable conditions for further distortion. Second, a greater electronegativity difference between the ligand and the central atom promotes band expansion and reduces the negative impact of TMs on the bandgap.[25,26] Based on these principles, we identified $NH_2SO_3^-$ containing mixed anions with strong electronegativity as the optimal X-site ligand. Additionally, $NH_2SO_3^-$ features ultra-large HOMO–LUMO gaps (approximately 8.17 eV),[27] which should be conducive to further expanding the band gap.[28,29]

Furthermore, ensuring the geometric stability of the perovskite structure is paramount, as excessive octahedral distortion can result in structural instability. The octahedral factor (μ) and tolerance factor (t) play crucial roles in evaluating structural stability: stable octahedral formations necessitate a range of $0.44 < \mu < 0.90$.[30] In light of this, we chose Cd^{2+} ($\mu = 0.48$) as the B-site cation, as Zn^{2+} ($\mu = 0.37$) could potentially lead to structural collapse. The tolerance factor, t, serves as an indicator of structural behavior, where a range of $0.89 < t < 1.00$ indicates a stable cubic phase. When t is in the range of 0.81 to 0.89, the cubic phase structure can distort into lower-symmetry space groups while maintaining overall structural stability, while $t < 0.81$ suggests the possibility of collapse.[31,32] Notably, the cubic phase is unsuitable for NLO applications due to its lack of birefringence. Therefore, we identified K (t = 0.88) as the most appropriate A-site cation for NLO materials, ensuring both structural stability and the desired optical properties.

Consequently, with these considerations in mind, we successfully synthesized a novel perovskite-type crystal, polyhedral $(NH_2SO_3)_3$, exhibiting a substantial SHG response and a short UV cut-off edge enabling DUV access. Notably, this material can be easily grown using a simple aqueous solution evaporation method, yielding large single crystals measuring 20 × 17 × 5 mm^3. This breakthrough elegantly reconciles the challenge between achieving strong SHG and a short UV absorption edge, thereby setting a new paradigm for the design of DUV NLO materials.

Experimental section

Reagents

H_2O, KOH (Adamas, ≥99.9%), $CdCO_3$ (Adamas, 99.9%), and HSO_3NH_2 (Adamas, 99.0%) were used to grow the perovskite-type crystals.

Single-crystal growth

First, 0.1 mol each of KOH and $CdCO_3$, and 0.3 mol of NH_3SO_3 were weighed, following a 1 : 3 stoichiometric ratio. The beaker was placed on a temperature-controlled heated magnetic stirrer, dissolving NH_3SO_3 in 300 ml of water at 50 °C. Once dissolved, KOH and $CdCO_3$ were gradually added. The mixture was allowed to react for 2 hours, and then the solution was filtered. Next, the filtered solution was put in an oven at 50 °C for evaporation. When crystal grains were formed, the solution was transferred to a 50 °C water bath and cooled at 0.5 °C per day to grow crystals. As the temperature reached 40 °C, the reduced solute concentration slowed down crystal growth, and impurity ions increased, causing defects. At this stage, the crystals were removed.

Single-crystal X-ray diffraction

A PXS5-B1 continuous zoom stereo microscope was used to meticulously select colorless $KCd(NH_2SO_3)_3$ crystals. The crystal structure of $KCd(NH_2SO_3)_3$ was determined using single-crystal X-ray diffraction data collected with a Rigaku Mercury CCD diffractometer and graphite-monochromated Mo-Kα radiation (λ = 0.7103 Å). Additionally, the structure was solved using direct methods in OLEX2 with the SHELXTL program.[33,34]

Power X-ray diffraction

The grown small crystals were ground into very fine powder and spread evenly on a glass slide specifically designed for testing. To obtain the powder X-ray diffraction data of $KCd(NH_2SO_3)_3$ using Cu Kα radiation (λ = 1.540598 Å), the test 2θ range was set from 5° to 60°, the scan step width at 0.01° and the scan speed at 0.1° min^{-1}.

Energy-dispersive X-ray spectroscopy analysis

Microprobe elemental analyses were performed on a field emission scanning electron microscope (FESEM, SU-8010) equipped with an energy dispersive X-ray spectrometer (EDS).

Thermogravimetric analysis (TGA)

Thermogravimetric analysis (TGA) was conducted using a Netzsch STA449F3 simultaneous analyzer under flowing N_2 at a heating rate of 10 °C min^{-1}.

Optical properties

At room temperature, the UV-vis-NIR transmission spectral data of $KCd(NH_2SO_3)_3$, following a polishing process, were recorded by scanning in the wavelength range of 190–800 nm using a Lambda 950 UV-vis-NIR spectrophotometer (PerkinElmer).

Second-harmonic generation measurements

The polycrystalline SHG signals for $KCd(NH_2SO_3)_3$ were measured on a 1064 nm solid-state laser with KDP crystals as reference samples. The crystals were ground and sieved into six different sizes: 25–45 μm, 45–62 μm, 62–75 μm, 75–109 μm, 109–150 μm, and 150–212 μm.

Theoretical calculations

Density functional theory (DFT)[35] calculations were performed to determine the band structure of $KCd(NH_2SO_3)_3$. The exchange–correlation energy was modeled using the generalized gradient approximation (GGA) with the Perdew–Burke–Ernzerhof (PBE)[36] functional. The valence electron configurations considered were as follows: K ($3s^2$ $3p^6$ $4s^1$), Cd ($4d^{10}$ $5s^2$), S ($3s^2$ $3p^4$), O ($2s^2$ $2p^4$), N ($2s^2$ $2p^3$), and H ($1s^1$). A plane-wave energy cutoff of 600 eV was applied, and the reciprocal space was sampled with a 2 × 2 × 2 Monkhorst–Pack grid. The HSE06 hybrid functional was employed to refine the band gap and density of states (DOS) calculations for $KCd(NH_2SO_3)_3$. Nonlinear optical (NLO) coefficients (d_{ij}) were computed using the method proposed by Rashkeev *et al.*, with further developments by Lin *et al.*[37] The dipole was calculated with the B3LYP/def2svp method implemented by Gaussian 09.

Results and discussion

A high-quality, colorless, and transparent single crystal of $KCd(NH_2SO_3)_3$ was successfully grown *via* an aqueous solution method, reaching dimensions of up to 20 × 17 × 5 mm^3 (Fig. S1†). The crystal quality was further assessed through high-resolution X-ray diffraction, with the full width at half maximum (FWHM) of the rocking curve measured at 93.6″ (Fig. S2†) being indicative of its high quality. The powder X-ray diffraction (XRD) patterns exhibited excellent agreement with simulated patterns derived from the crystal structure, confirming the phase purity (Fig. S3†). Energy-dispersive X-ray spectroscopy (EDS) analysis revealed the presence of K, Cd, N, S, and O elements in the crystal, with atomic ratio analysis indicating a stoichiometric ratio of K : Cd : N : S : O of approximately 1 : 1 : 3 : 3 : 9 (Fig. S4†), consistent with the chemical formula. Notably, the crystal maintained its transparency even after exposure to air for several months. Thermal analysis demonstrated excellent thermal stability, with the crystal remaining stable up to 210 °C (Fig. S5†), comparable to most reported sulfamic NLO crystals.[27–29]

The crystal structure of $KCd(NH_2SO_3)_3$, as depicted in Fig. 1(a) and (b), belongs to the non-centrosymmetric hexagonal space group $P6_3$ (no. 173). In this structure, a significantly polar $[CdN_3O_3]$ octahedron is formed, where three N atoms and O atoms are located on opposite sides, leading to differences in bond lengths. Adjacent octahedra are interconnected by sharing $SO_3NH_2^-$ with dipole moments of all octahedra uniformly aligned along the *c*-axis, thus forming a non-centrosymmetric structural framework. To maintain charge balance

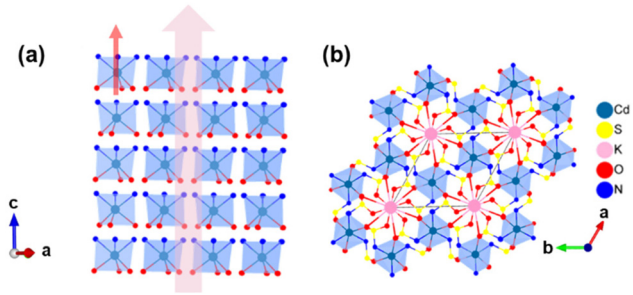

Fig. 1 (a) The dipole moment of $KCd(NH_2SO_3)_3$ along the *c*-axis; and (b) the 3D crystal structure of $KCd(NH_2SO_3)_3$ in the *a*–*b* plane.

within this framework, K^+ ions fill the gaps, resulting in the three-dimensional crystal structure of $KCd(NH_2SO_3)_3$.

The transformation from the classic cubic perovskite structure ABX_3 to $KCd(NH_2SO_3)_3$ is depicted in Fig. 2 and can be understood through a strategic three-step structural design approach. (1) *Inducing octahedral distortion and bandgap expansion*: To create a distorted octahedron while widening the bandgap, $NH_2SO_3^-$ was selected as the X-site in the BX_6 unit. The presence of highly electronegative N and O atoms provides varied coordination environments for the B-site cation, facilitating distortion. Additionally, the large HOMO–LUMO gap of $NH_2SO_3^-$ (approximately 8.17 eV)[27] contributes to an extensive ultraviolet transparency window for the material. (2) *Stabilizing the octahedral model and avoiding red shift*: The selection of the B-site ion is crucial for forming a stable $B(NH_2SO_3)_6$ octahedral configuration with $NH_2SO_3^-$ while preventing the cutoff edge red shift associated with the second-order Jahn–Teller effect in d^0 metals. Using the octahedral factor calculation, Cd^{2+} (μ = 0.48) was chosen from d^{10} metals as the B-site cation. Both N and O atoms in $NH_2SO_3^-$ can form covalent bonds with Cd^{2+}, resulting in a distorted $[CdN_3O_3]$ octahedral unit with Cd–O and Cd–N bond lengths of 2.303(4) Å and 2.371(5) Å, respectively. As each atom originates from the tetrahedral $NH_2SO_3^-$, the eventual BX_6 unit formed is $Cd(NH_2SO_3)_6$. (3) *Ensuring structural stability and crystal system modification*: To ensure the stability of the $ACd(NH_2SO_3)_3$ structure and avoid crystallization in a non-birefringent cubic crystal system, K (t = 0.88) was selected as the A-site cation. This choice was guided by electroneutrality principles and tolerance factor calculations (Fig. 3). The reduction in the tolerance factor facilitates the transition of the cubic perovskite of ABX_3 into a monoclinic phase, thus enabling changes in the crystal system. Ultimately, $KCd(NH_2SO_3)_3$ was realized on the perovskite framework, maintaining the quintessential ABX_3 structure.

The ultraviolet transmission spectrum of $KCd(NH_2SO_3)_3$ reveals an exceptionally short UV cutoff edge below 190 nm (Fig. 4a), corresponding to a large bandgap of 6.5 eV, which is in excellent agreement with the HSE06-calculated value of 6.22 eV (Fig. S6†). According to the anionic group theory, the formation of a large bandgap is primarily attributed to the HOMO–LUMO gap of the group. Our calculations on $NH_2SO_3^-$ reveal a HOMO–LUMO gap of approximately 8.17 eV, signifi-

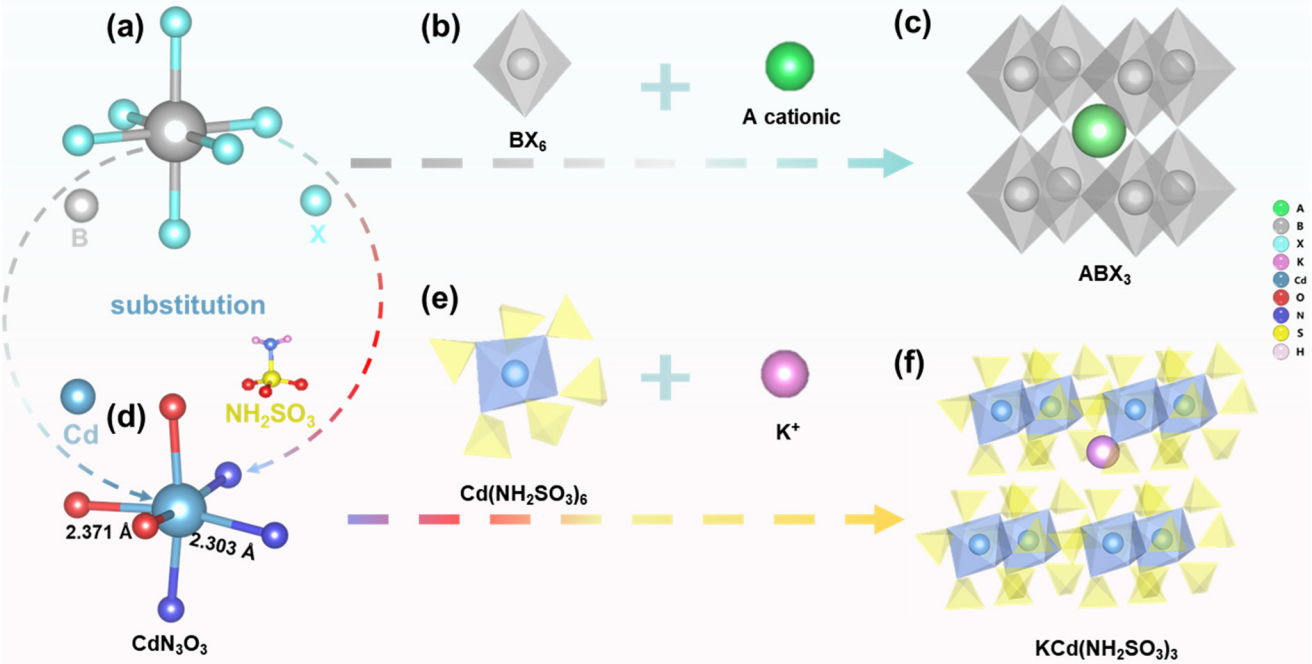

Fig. 2 (a) The BX_6 ball-and-stick model; (b) BX6 octahedron; (c) the perovskite ABX_3 cubic framework; (d) the CdN_3O_3 ball-and-stick model; (e) Cd $(NH_2SO_3)_6$ as a combination of octahedral and tetrahedral structures in the BX_6 unit; and (f) the $KCd(NH_2SO_3)_3$ monoclinic prismatic distorted perovskite framework.

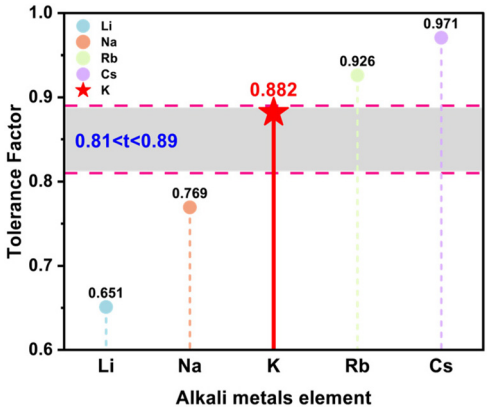

Fig. 3 The tolerance factor for each alkali metal (Li, Na, K, Rb, and Cs) and the maintained reasonable range for phase transition and structural stability.

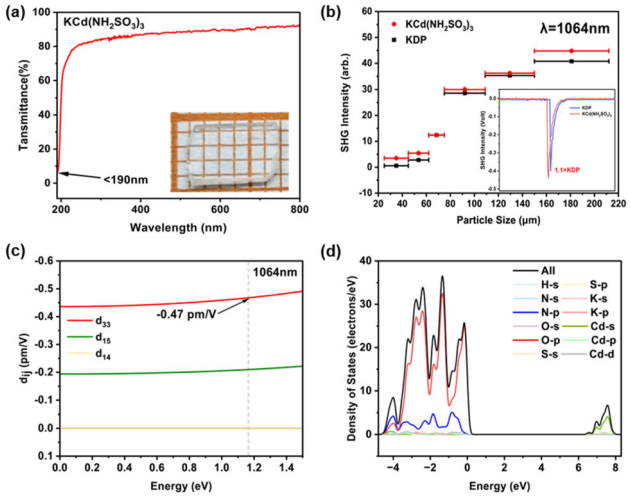

Fig. 4 (a) The UV/vis diffuse-reflectance spectrum of $KCd(NH_2SO_3)_3$; the inset shows the wafers used for testing. (b) Powder SHG measurement at 1064 nm. (c) Calculated SHG coefficients of $KCd(NH_2SO_3)_3$. (d) PDOS analysis for $KCd(NH_2SO_3)_3$.

cantly larger than 6.5 eV, indicating that sulfamate salts possess a distinct advantage of wide ultraviolet transmittance. This is further corroborated by a series of examples of sulfamate salts.

To gain insight into the mechanism underlying the formation of this large bandgap, we further calculated the projected density of states (PDOS). As shown in Fig. 4d, the conduction band minimum of $KCd(NH_2SO_3)_3$ is predominantly composed of Cd-s states, while the valence band maximum is jointly occupied by O-p and N-p states, suggesting that the bandgap is primarily determined by the $Cd(NH_2SO_3)_6$ octahedron. Notably, our previous studies have shown that the $-NH_2$ group exhibits a stronger electron-withdrawing effect compared to O, which may effectively confine the electron cloud around Cd, resulting in bandgap widening. This is likely the primary reason for the large bandgap in $KCd(NH_2SO_3)_3$.

The non-centrosymmetric structure of $KCd(NH_2SO_3)_3$ encouraged us to explore its SHG properties using the Kurtz–Perry method,[38] with KDP as a reference sample. As

depicted in Fig. 4b, $KCd(NH_2SO_3)_3$ exhibited distinct phase-matching characteristics during frequency doubling from 1064 nm to 532 nm, accompanied by a significant SHG effect (1.1 × KDP). Theoretical calculations revealed that the largest NLO coefficient, d_{33}, is −0.47 pm V^{-1}, which is 1.2 times that of KDP (0.39 pm V^{-1}), closely corroborating the experimental results. To elucidate the mechanism underlying its NLO coefficient, we calculated the SHG density map. As shown in Fig. S7,† the SHG density is predominantly concentrated around Cd^{2+} and $SO_3NH_2^-$, indicating that the SHG effect is mainly attributed to the $[Cd(NH_2SO_3)_6]$ octahedra, whereas the K^+ ions contribute negligibly. We have compiled most of the known UV/DUV Cd-based NLO materials, as shown in Table S6.† To the best of our knowledge, this may be the largest crystal size grown for a Cd-based DUV NLO material with large SHG effects.

To further elucidate the impact of octahedral distortion on SHG, we performed theoretical calculations on the degree of distortion, dipole moment, and hyperpolarizability of the octahedron. The standard deviation method ($\xi = \sqrt{\frac{1}{12}\sum_{i=1}^{12}(L_i - \bar{L})^2}$, where L_i is the edge length of the octahedron, and $\bar{L}$ is the average value of the edge lengths) was employed to quantify the degree of distortion, as shown in Fig. S8,† when the three O–Cd–N bond angles increased from 169.007° to 180°. Also, as calculated from the data in Fig. S8† using the above formula, the degree of distortion decreased from 0.2174 to 0.0482. Concomitantly, the dipole moment decreased from 7.5713 D to 6.96 D, and the hyperpolarizability decreased from 667.01 to 512.71 (Table S5†). These findings clearly demonstrate that reducing the degree of distortion diminishes the polarity of the octahedron and corresponds to a decrease in hyperpolarizability. In contrast, an increase in the degree of distortion contributes to the enhancement of hyperpolarizability, leading to improved SHG response, which is in line with our design concept. Notably, the arrangement of units also plays a crucial role in the SHG effect of NLO crystals. In the case of $KCd(NH_2SO_3)_3$, the consistent alignment of $[CdN_3O_3]$ octahedra results in a dipole moment of 17.6877 D along the *c*-axis, and the uniform arrangement of distorted octahedra provides favorable conditions for large SHG effects.

Conclusions

In conclusion, we have successfully designed and synthesized a novel non-centrosymmetric compound, $KCd(NH_2SO_3)_3$, based on a perovskite framework. Notably, this material exhibits a desirable balance of properties, featuring a deep ultraviolet (DUV) absorption edge shorter than 190 nm and a strong second-harmonic generation (SHG) response of 1.1 × KDP. These excellent properties can be attributed to the synergistic effect of distorted $[CdO_3N_3]$ octahedra and $SO_3NH_2^-$ groups. Furthermore, we have successfully grown large, high-quality crystals, achieving a transparent single crystal with dimensions of 20 × 17 × 5 mm^3. The combination of excellent optical properties and good growth habits makes $KCd(NH_2SO_3)_3$ a promising new candidate for DUV nonlinear optical (NLO) crystals. More importantly, our design approach provides a new and feasible method for exploring DUV NLO crystals, opening up new avenues for the development of advanced optical materials.

Data availability

The authors confirm that the data supporting the findings of this study are available within the article [and/or its ESI†].

Conflicts of interest

There are no conflicts to declare.

Acknowledgements

This work was supported by the National Natural Science Foundation of China (22471271, 22222510, 21921001, 52302008); the Natural Science Foundation of Fujian Province (2023J02026); the Self-deployment Project Research Program of Haixi Institutes, Chinese Academy of Science (CXZX-2022-JQ01, CXZX-2022-GH06), and the Youth Innovation Promotion Association CAS (Y2023082).

References

1 D. Cyranoski, A Chinese laboratory is the only source of a valuable crystal, *Nature*, 2009, **457**, 953–955.
2 M. Mutailipu, M. Zhang, Z. Yang and S. Pan, Targeting the next generation of deep-ultraviolet nonlinear optical materials: expanding from borates to borate fluorides to fluorooxoborates, *Acc. Chem. Res.*, 2019, **52**, 791–801.
3 C. T. Chen, G. L. Wang, X. Y. Wang and Z. Y. Xu, Deep-UV nonlinear optical crystal $KBe_2BO_3F_2$—discovery, growth, optical properties and applications, *Appl. Phys. B*, 2009, **97**, 9–25.
4 M. Luo, Compounds Consisting of Coplanar π-conjugated B_3O_6 typed Structures: An Emerging Source of Ultraviolet Nonlinear Optical Materials, *J. Sichuan Norm. Univ., Nat. Sci.*, 2024, **47**(1), 1–16.
5 C. Wu, G. Yang, M. G. Humphrey and C. Zhang, Recent advances in ultraviolet and deep-ultraviolet second-order nonlinear optical crystals, *Coord. Chem. Rev.*, 2018, **375**, 459–488.
6 L. Kang and Z. Lin, Deep-ultraviolet nonlinear optical crystals: concept development and materials discovery, *Light: Sci. Appl.*, 2022, **11**, 201.
7 M. Mutailipu and S. Pan, Emergent deep–ultraviolet nonlinearoptical candidates, *Angew. Chem., Int. Ed.*, 2020, **59**, 20302–20317.

8 H. Yu, N. Z. Koocher, J. M. Rondinelli and P. S. Halasyamani, Pb $_2$ BO $_3$ I: a borate iodide with the largest second–harmonic generation (SHG) response in the $KBe_2BO_3F_2$ (KBBF) family of nonlinear optical (NLO) materials, *Angew. Chem.*, 2018, **130**, 6208–6211.
9 M. A. Peña and J. L. G. Fierro, Chemical structures and performance of perovskite oxides, *Chem. Rev.*, 2001, **101**, 1981–2018.
10 M. Ahmadi, T. Wu and B. Hu, A review on organic–inorganic halide perovskite photodetectors: Device engineering and fundamental physics, *Adv. Mater.*, 2017, **29**, 1605242.
11 J. Hwang, R. R. Rao, L. Giordano, Y. Katayama, Y. Yu and Y. Shao-Horn, Perovskites in catalysis and electrocatalysis, *Science*, 2017, **358**, 751–756.
12 M. Capdevila-Cortada, Describing perovskite catalysts, *Nat. Catal.*, 2018, **1**, 737–737.
13 F. P. García De Arquer, A. Armin, P. Meredith and E. H. Sargent, Solution-processed semiconductors for next-generation photodetectors, *Nat. Rev. Mater.*, 2017, **2**, 16100.
14 Y. Maeno, H. Hashimoto, K. Yoshida, S. Nishizaki, T. Fujita, J. G. Bednorz and F. Lichtenberg, Superconductivity in a layered perovskite without copper, *Nature*, 1994, **372**, 532–534.
15 S. H. Wemple, M. Didomenico and I. Camlibel, Dielectric and optical properties of melt-grown $BaTiO_3$, *J. Phys. Chem. Solids*, 1968, **29**, 1797–1803.
16 G. D. Boyd, R. C. Miller, K. Nassau, W. L. Bond and A. Savage, $LiNbO_3$: An Efficient Phase Matchable Nonlinear Optical Material, *Appl. Phys. Lett.*, 1964, **5**, 234–236.
17 A. Bruner, D. Eger, M. B. Oron, P. Blau, M. Katz and S. Ruschin, Temperature-dependent sellmeier equation for the refractive index of stoichiometric lithium tantalate, *Opt. Lett.*, 2003, **28**, 194.
18 P. S. Halasyamani, Asymmetric cation coordination in oxide materials: influence of lone-pair cations on the intra octahedral distortion in d^0 transition metals, *Chem. Mater.*, 2004, **16**, 3586–3592.
19 Z. Y. Bai and K. M. Ok, Advances in aliovalent substitution strategy for the design and synthesis of nonlinear optical materials: D^0 transition metal/gallium iodates and selenites, *Coord. Chem. Rev.*, 2023, **490**, 215212.
20 S. Zhao, J. Zhang, S. Zhang, Z. Sun, Z. Lin, Y. Wu, M. Hong and J. Luo, A new UV nonlinear optical material $CsZn_2B_3O_7$:ZnO_4 tetrahedra double the efficiency of second-harmonic generation, *Inorg. Chem.*, 2014, **53**, 2521–2527.
21 H. Yu, W. Zhang, J. Young, J. M. Rondinelli and P. S. Halasyamani, Design and synthesis of the beryllium–free deep–ultraviolet nonlinear optical material Ba_3 (ZnB_5O_{10})PO_4, *Adv. Mater.*, 2015, **27**, 7380–7385.
22 Y.-G. Chen, M.-L. Xing, P.-F. Liu, Y. Guo, N. Yang and X.-M. Zhang, Two phosphates: Noncentrosymmetric $Cs_6Mg_6(PO_3)_{18}$ and centrosymmetric $Cs_2MgZn_2(P_2O_7)_2$, *Inorg. Chem.*, 2017, **56**, 845–851.
23 Y. G. Shen, S. G. Zhao, B. Q. Zhao, C. M. Ji, L. N. Li, Z. H. Sun, M. C. Hong and J. H. Luo, Strong nonlinear-optical response in the pyrophosphate $CsLiCdP_2O_7$ with a short cutoff edge, *Inorg. Chem.*, 2016, **55**, 11626–11629.
24 C. Furlani, Ligand field interpretation of some cases of pentacoordination, *Coord. Chem. Rev.*, 1968, **3**, 141–167.
25 P. F. Zhu, P. F. Gong, Z. Y. Wang, H. T. Jiang, J. F. Zhao, C. Li, Z. S. Lin, X. L. Duan and F. P. Yu, Enlargement of bandgap and birefringence in nonlinear optical alkali–metal sulfate crystals by the substitution of asymmetrical non–π–conjugated cation, *Adv. Opt. Mater.*, 2023, **11**, 2301152.
26 Y. L. Hu, C. Wu, X. X. Jiang, K. N. Duanmu, Z. P. Huang, Z. S. Lin, M. G. Humphrey and C. Zhang, Ultrashort phase–matching wavelength and strong second–harmonic generation in deep–UV–transparent oxyfluorides by covalency reduction, *Angew. Chem., Int. Ed.*, 2023, **62**, e202315133.
27 X. Hao, M. Luo, C. Lin, G. Peng, F. Xu and N. Ye, Two deep–ultraviolet transparent sulfamates exhibiting strong second harmonic generation responses and moderate birefringence, *Angew. Chem., Int. Ed.*, 2021, **60**, 7621–7625.
28 X. F. Wang, X. D. Leng, Y. Kuk, J. Lee, Q. Jing and K. M. Ok, Deep–ultraviolet transparent mixed metal sulfamates with enhanced nonlinear optical properties and birefringence, *Angew. Chem., Int. Ed.*, 2024, **63**, e202315434.
29 H. Tian, N. Ye and M. Luo, Sulfamide: a promising deep–ultraviolet nonlinear optical crystal assembled from polar covalent [$SO_2(NH_2)_2$] tetrahedra, *Angew. Chem., Int. Ed.*, 2022, **61**, e202200395.
30 M. A. Green, A. Ho-Baillie and H. J. Snaith, The emergence of perovskite solar cells, *Nat. Photonics*, 2014, **8**, 506–514.
31 R. D. Jolly, Mannosidosis of angus cattle: a prototype control program for some genetic diseases, *Adv. Vet. Sci. Comp. Med.*, 1975, **19**, 1–21.
32 Y. Xin, D. Yan-Li, Z. Xiao-Dan, Z. Ying and Institute of Photo Electronics Thin Film Devices and Technology of Nankai University, Tianjin 300071, China, A review of the perovskite solar cells, *Acta Phys. Sin.*, 2015, **64**, 38805.
33 G. M. Sheldrick, A short history of SHELX, *Acta Crystallogr., Sect. A: Found. Crystallogr.*, 2008, **64**, 112–122.
34 D. Chernyshov, V. Dyadkin and K. W. Törnroos, Sequential Shelxl Refinement of Consecutive Datasets: A Tool to Probe Dynamically Evolving Single Crystal Structures, *Acta Crystallogr., Sect. A:Found. Adv.*, 2019, **75**, e678–e678.
35 A. M. Rappe, K. M. Rabe, E. Kaxiras and J. D. Joannopoulos, Optimized pseudopotentials, *Phys. Rev. B: Condens. Matter Mater. Phys.*, 1990, **41**, 1227–1230.
36 J. P. Perdew, K. Burke and M. Ernzerhof, Generalized Gradient Approximation Made Simple, *Phys. Rev. Lett.*, 1997, **78**, 1396–1396.
37 W.-D. Cheng, C.-S. Lin, H. Zhang and G.-L. Chai, Theoretical Evaluation on Terahertz Source Generators from Ternary Metal Chalcogenides of PbM_6Te_{10} (M = Ga, In), *J. Phys. Chem. C*, 2018, **122**, 4557–4564.
38 S. K. Kurtz and T. T. Perry, A powder technique for the evaluation of nonlinear optical materials, *J. Appl. Phys.*, 1968, **39**, 3798–3813.